Millimeter-wave spectroscopy and multichannel quantum-defect-theory analysis of high Rydberg states of krypton: The hyperfine structure of $^{83}Kr^+$

Martin Schäfer and Frédéric Merkt*
Laboratorium für Physikalische Chemie, ETH Zürich, CH-8093 Zurich, Switzerland
(Received 6 September 2006; published 8 December 2006)

The intervals between hyperfine levels of high *ns* and *nd* ($n=68-76$) Rydberg states of ^{83}Kr have been determined by millimeter-wave spectroscopy. The hyperfine structure of the Rydberg states has been analyzed using multichannel quantum defect theory. Improved eigenquantum defects for the *ns* and *nd* Rydberg series and quantitative information about the *s*-*d* interaction at the energy of the $^2P_{3/2}$ threshold have been obtained, and improved values of the hyperfine structure of the $^2P_{3/2}$ ground state of $^{83}Kr^+$ have been derived.

DOI: 10.1103/PhysRevA.74.062506 PACS number(s): 32.10.Fn, 32.80.Rm, 32.30.Bv, 34.60.+z

I. INTRODUCTION

The determination of high-resolution spectroscopic information of cations represents a considerable challenge, particularly in cases where no allowed transitions lie in the infrared and visible regions of the electromagnetic spectrum. In such cases the information on the cation can be derived from Rydberg state spectroscopy and extrapolation of the Rydberg series using multichannel quantum defect theory (MQDT). This method has been recently used to determine the hyperfine structure of the ground state of ortho-H_2^+ [1] and its application to the determination of the hyperfine structure of the $^2P_{3/2}$ ground state of $^{83}Kr^+$ is described here.

The development of narrow-bandwidth vacuum-ultraviolet (vuv) laser systems has made it possible to resolve the hyperfine structure of high Rydberg states following excitation from the neutral ground state [2–6]. A much higher spectral resolution can be achieved by using millimeter wave spectroscopy of high-*n* Rydberg states in combination with selective field ionization [7–9]. This technique has been used to measure the properties of Rydberg states of sodium [7,10,11], argon [12], krypton [13–15], benzene [16], and H_2 [1,17] at principal quantum numbers $n>20$ and submegahertz resolution. Millimeter- and submillimeter-wave sources for spectroscopic measurements on Rydberg states in the 118–180 GHz and 240–380 GHz frequency ranges have been described in Refs. [12,15].

A large body of experimental data exists on the gerade and ungerade Rydberg states of krypton [2,3,5,15,18–35] and multichannel quantum defect theory analyses of these states have been reported [25,31,36–44]. The available sets of quantum defects and channel interaction parameters describe the rich photoionization dynamics of krypton, but so far only few isotope-selective studies have been reported. The parameters describing the interactions between *s* and *d* ionization channels, which are important to describe the autoionization dynamics of the rare gas atoms [45], remain uncertain and ambiguities concerning the energy dependence of the MQDT parameters persist.

In a recent high-resolution vuv laser spectroscopic study of ^{83}Kr, an avoided crossing between hyperfine levels of $(n+2)s$ and *nd* Rydberg states was observed around $n=70$ [5]. In the same study, an MQDT formalism to analyze the hyperfine structure of Rydberg states of krypton was developed but the experimental resolution of 250 MHz, although sufficient to partially resolve the hyperfine structure of *s* and *d* Rydberg levels, was not sufficient to derive unambiguous *s*-*d* interaction parameters.

The present study describes a measurement, by millimeter-wave spectroscopy, of the level structure of *s* and *d* Rydberg states of ^{83}Kr and ^{84}Kr between $n=68$ and 74. This measurement was carried out to obtain information on the interaction between *s* and *d* channels in krypton manifested by perturbations of the hyperfine structure in the spectra of ^{83}Kr and to derive, in an MQDT analysis, the hyperfine structure of the $^2P_{3/2}$ ground state of Kr^+ with a precision of better than 1 MHz. The MQDT analysis focuses on the region of high-*n* Rydberg states below the $^2P_{3/2}$ ionization limit, and relies on the use of μ quantum defects [46,47], and therefore does not provide additional information on the energy dependence of the MQDT parameters. The energy dependence of the MQDT parameters for all $J=0-4$ channels will be discussed in a forthcoming publication [48] in which a global fit of the present experimental data and of all data available in the literature on all isotopes of krypton will be described and a detailed comparison of μ and η quantum defects will be presented.

II. EXPERIMENTS

The millimeter-wave spectra of high-*n* Rydberg states of krypton were measured in an experiment similar to that described in Ref. [12]. A detailed description of the millimeter-wave source, a phase-stabilized backward wave oscillator operating in the frequency range 240–380 GHz, is given in Ref. [15].

A tunable, pulsed vuv laser [49] (0.1 cm^{-1} bandwidth) was used to induce a transition from the $(4p)^6\,{}^1S_0$ ground state to the $(4p)^5(^2P_{3/2})4d[1/2]_1$ state of krypton (97 085.19 cm^{-1}). The vuv radiation was produced by resonant two-color sum-frequency mixing ($\nu_{vuv}=2\nu_1+\nu_2$) in xenon using two neodymium-doped yttrium aluminum garnet-(Nd:YAG-)pumped dye lasers, the wave number of the first one doubled and set to correspond to the $6p[1/2]_0 \leftarrow {}^1S_0$

*Electronic address: merkt@xuv.phys.chem.ethz.ch

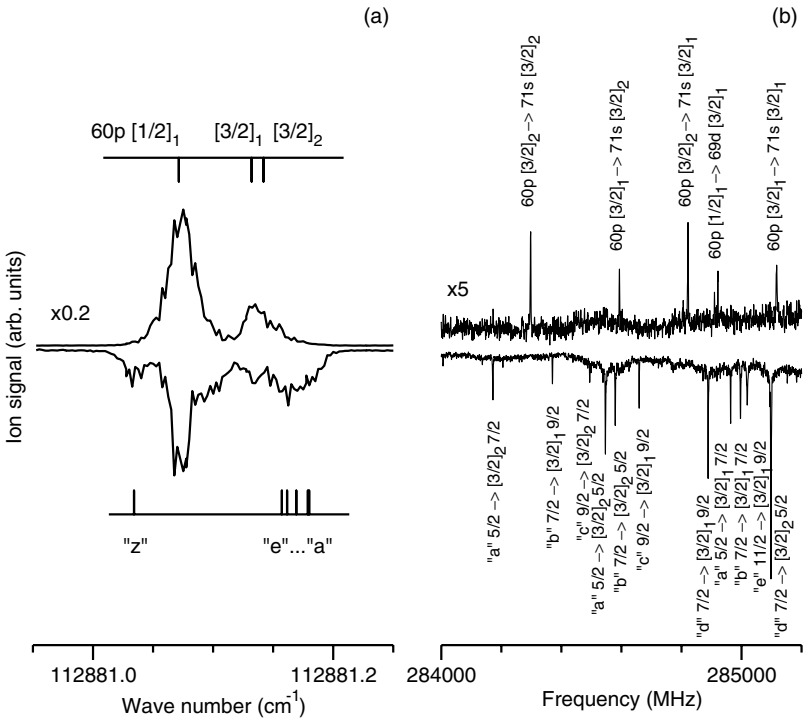

FIG. 1. (a) shows the pulsed-field-ionization spectra of the $60p$ Rydberg states of ^{84}Kr (upper trace) and ^{83}Kr (lower, inverted trace). Note that the ^{84}Kr signal is slightly leaking into the ^{83}Kr mass channel. Assignment bars indicate the positions of the levels probed by millimeter-wave spectroscopy (see Table I). (b) shows a section of the millimeter-wave spectra of the $71s \leftarrow 60p$ transitions of ^{84}Kr (upper trace) and ^{83}Kr (lower, inverted trace) when the tunable dye laser was set to excite the high-frequency end of the $60p$ state (in the range of the levels "a"–"e" of ^{83}Kr).

two-photon resonance of xenon ($2\nu_1 = 80\,118.97\ \mathrm{cm}^{-1}$). The sum-frequency radiation was separated from the fundamental laser radiation and from radiation generated by other nonlinear processes in a differentially pumped vacuum monochromator equipped with a toroidal grating, which recollimated the diverging vuv beam and directed it toward the photoexcitation chamber. A pulsed skimmed supersonic beam of krypton (Pangas, spectroscopic grade purity) crossed the vuv laser beam at right angles in the middle of an array of resistively coupled cylindrical extraction plates. A third tunable dye laser, operated with intracavity étalon and pumped by the same Nd:YAG laser, was used to excite krypton from the $4d[1/2]_1$ intermediate state into high np Rydberg states ($n \geqslant 58$), which served as initial states for millimeter-wave transitions. Figure 1(a) shows, as an example, the spectrum in the region of the $n=60$ p manifold of states. The beam of the third dye laser and the millimeter-wave radiation entered the photoexcitation region in opposite directions perpendicular to the vuv laser and the krypton gas beam. The millimeter-wave transitions were detected by selective field ionization using a pulsed electric field (30–40 V/cm), which was applied 1–4 μs after the laser pulse and also accelerated the krypton ions toward a microchannel plate (MCP) detector. Spectra of different krypton isotopes (^{84}Kr, ^{83}Kr) were obtained by placing temporal gates at the corresponding positions of the time-of-flight spectrum and examples of such spectra are displayed in Fig. 1(b). The photoexcitation region and the adjacent time-of-flight tube were surrounded by two cylindrical mu-metal shields to minimize stray magnetic fields. The residual stray electric fields were reduced to below 5 mV/cm using the procedure described in [14] so that an accuracy in the measured transition frequencies of better than 1 MHz was achieved. The procedure, illustrated in Fig. 2(a), consisted of measuring the Stark shift for different applied fields and determining the field for which the Stark shift was minimal.

In order to avoid power broadening of the millimeter-wave transitions (cf. Ref. [12]), the millimeter-wave radiation was attenuated by about −10 dB by introducing stacks of paper between the millimeter-wave source and the experimental chamber. In most spectra the resolution was limited by the measurement time, i.e., either the time between the laser excitation pulse and the field ionization pulse or the transit time of the excited atoms through the region of the interaction with the millimeter waves [9]. Using a time delay of 4 μs between laser pulse and field ionization pulse, lines as narrow as 220 kHz were observed [see Fig. 2(b)].

III. MQDT CALCULATIONS

To analyze the Rydberg spectrum of Kr using MQDT, we follow the formalism introduced by Lu [50] and Lee and Lu [51] for the analysis of the Xe and Ar absorption spectra. This formalism was used by Aymar and co-workers [39] to treat the $J=0$–4 odd-parity bound Rydberg states of Kr, and was extended by Wörner *et al.* [5] for the analysis of the hyperfine structure of ^{83}Kr in a method similar to that outlined by Sun [52].

For atoms with a nuclear spin $I=0$, the energies of the bound states are well described by a set of MQDT parameters consisting of the ionization thresholds $E(^2P_{J^+})$, the eigenchannel quantum defects μ_α, their energy dependence, and the elements of the orthogonal transformation matrix $U_{i\alpha}$ connecting the close-coupling eigenchannels α (which are well described by the LS coupling scheme) to the fragmentation channels i, which are jj coupled. Each bound energy level is represented by two effective principal quantum numbers $\nu_{3/2}$ and $\nu_{1/2}$ defined by the relations

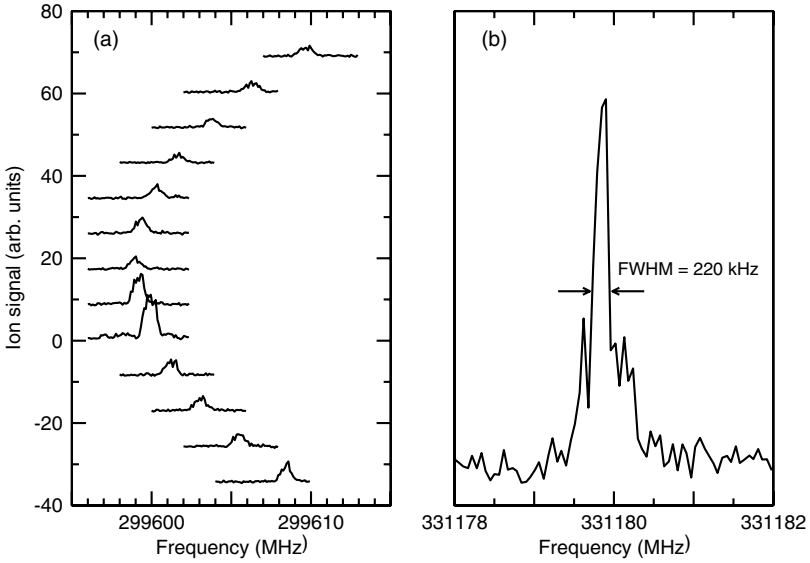

FIG. 2. (a) shows the millimeter-wave spectra of the $70d\ [1/2]_1 \leftarrow 60p\ [1/2]_1$ transition of ^{84}Kr in the presence of different electric fields. The spectra have been shifted along the vertical axis by an offset corresponding to the value of the applied field in mV/cm (top spectrum 69.0 mV/cm, bottom spectrum −34.5 mV/cm). (b) shows the millimeter-wave spectrum of the $68d\ [5/2]_2\ (F=5/2) \leftarrow 58p$ "b" $(F=7/2)$ transition of ^{83}Kr recorded using a delay time of 4 μs between laser pulse and pulsed field ionization.

$$E = E(^2P_{3/2}) - \frac{R_M}{\nu_{3/2}^2} = E(^2P_{1/2}) - \frac{R_M}{\nu_{1/2}^2}, \tag{1}$$

where R_M is the mass-dependent Rydberg constant. The bound energy levels are the solutions satisfying the relation

$$\det|U_{i\alpha} \sin[\pi(\mu_\alpha + \nu_i)]| = 0, \tag{2}$$

where ν_i is $\nu_{3/2}$ or $\nu_{1/2}$ for channels associated with the $^2P_{3/2}$ or $^2P_{1/2}$ ionization limits, respectively. The elements $U_{i\alpha}$ of the $N \times N$ transformation matrix are conveniently factorized as

$$U_{i\alpha} = \sum_{\bar{\alpha}} U_{i\bar{\alpha}} V_{\bar{\alpha}\alpha}, \tag{3}$$

where $U_{i\bar{\alpha}} = \langle LSJ|J^+ jJ\rangle$ represents elements of the *jj-LS* frame-transformation matrix, and $V_{\bar{\alpha}\alpha}$ accounts for the typically small departure of the close-coupling channels from pure *LS* coupling and may be represented by $N(N-1)/2$ generalized Euler angles θ_{jk} as described by Lee and Lu [51]:

$$V_{\bar{\alpha}\alpha} = \prod_{j}^{N} \prod_{k>j}^{N} \boldsymbol{R}(\theta_{jk}), \tag{4}$$

where $\boldsymbol{R}(\theta_{jk})$ are rotation matrices defined as

$$R_{mm}(\theta_{jk}) = \begin{cases} \cos\theta_{jk} & \text{if } m = j \text{ or } m = k, \\ 1 & \text{otherwise}, \end{cases}$$

$$R_{mn}(\theta_{jk}) = \begin{cases} -\sin\theta_{jk} & \text{if } m = j,\ n = k, \\ \sin\theta_{jk} & \text{if } m = k,\ n = j, \\ 0 & \text{otherwise}. \end{cases} \tag{5}$$

The energy dependence of μ_α can be approximated by

$$\mu_\alpha = \mu_\alpha^0 + \epsilon\mu_\alpha^1 \quad \text{with } \epsilon = 1/\nu_{3/2}^2; \tag{6}$$

a similar expression might be used for the energy dependence of $V_{\bar{\alpha}\alpha}$.

In the close-coupling region of the electron-ion collision, the electrostatic interaction between the electron and the ion core is much larger than the spin-orbit and the hyperfine interactions [51]. Therefore, the following angular momentum coupling scheme is adequate for the close-coupling eigenchannels:

$$\vec{L}^+ + \vec{\ell} = \vec{L}, \quad \vec{S}^+ + \vec{s} = \vec{S}, \quad \vec{L} + \vec{S} = \vec{J}, \quad \vec{J} + \vec{I} = \vec{F}, \tag{7}$$

where $\vec{L}^+$ and $\vec{S}^+$ represent the orbital and spin angular momenta of the ionic core, $\vec{\ell}$ and $\vec{s}$ the corresponding angular momenta of the Rydberg electron, and $\vec{I}$ the nuclear spin. In the long-range part of the electron-ion collision, however, the energy level structure of the Rydberg states corresponds primarily to the energy levels of the ionic core. Thus the following coupling scheme is used for the dissociation channels [5]:

$$\vec{L}^+ + \vec{S}^+ = \vec{J}^+, \quad \vec{J}^+ + \vec{I} = \vec{F}^+, \quad \vec{\ell} + \vec{s} = \vec{j}, \quad \vec{F}^+ + \vec{j} = \vec{F}. \tag{8}$$

Note that the assignments of the Rydberg levels observed in this study use the usual $n\ell[K]_J$ quantum numbers based on the following coupling scheme:

$$\vec{L}^+ + \vec{S}^+ = \vec{J}^+, \quad \vec{J}^+ + \vec{\ell} = \vec{K}, \quad \vec{K} + \vec{s} = \vec{J}, \quad \vec{J} + \vec{I} = \vec{F}. \tag{9}$$

Because the hyperfine interaction in the ionic core is much smaller than the spin-orbit interaction, which leads to an energy splitting of 5370.2 cm^{-1} between the $^2P_{3/2}$ and $^2P_{1/2}$ levels [23], mixing of the spin-orbit components by the hyperfine interaction is negligible. Therefore, the hyperfine structures of the two spin-orbit components can be treated separately and expressed as functions of the magnetic dipole and electric quadrupole constants A_{J^+} and B_{J^+} ($B_{1/2}=0$ for the $^2P_{1/2}$ spin-orbit level)

$$E(J^+,F^+) = E(J^+) + A_{J^+}\frac{C}{2} + B_{J^+}\frac{\frac{3}{4}C(C+1) - I(I+1)J^+(J^+ + 1)}{2I(2I-1)J^+(2J^+-1)}, \quad (10)$$

where $C=F^+(F^+ +1)-I(I+1)-J^+(J^+ +1)$ and $E(J^+)$ is the energy of the center of gravity of the hyperfine structure. The contribution from the octupole coupling is many orders of magnitude smaller [53] and thus neglected here. In analogy to Eq. (2), the Rydberg levels are determined by the determinantal equation

$$\det|U_{i_F\alpha_F}\sin[\pi(\mu_{\alpha_F} + \nu_{i_F})]| = 0, \quad (11)$$

where

$$U_{i_F\alpha_F} = \sum_{\bar{\alpha}_F} U_{i_F\bar{\alpha}_F} V_{\bar{\alpha}_F\alpha_F}, \quad (12)$$

and ν_{i_F} is an effective principal quantum number $\nu_{J^+F^+}$ defined relative to the position of the ionization threshold of the dissociation channel i_F (i.e., one of the six hyperfine levels of the ion):

$$E = E(^2P_{J^+F^+}) - \frac{R_M}{\nu^2_{J^+F^+}}. \quad (13)$$

The elements of the frame transformation matrix $U_{i_F\bar{\alpha}_F} = \langle LSJF|J^+F^+jF\rangle$ are calculated as [5]

$$\langle LSJF|J^+F^+jF\rangle = (2F+1)\sqrt{(2J+1)(2L+1)(2S+1)(2j+1)(2F^+ +1)(2J^+ +1)} \times \sum_{m_j,m_{J^+},m_J,m_\ell,m_{L^+},m_L,m_s,m_{S^+},m_S,m_{F^+},m_I} (-1)^{F^+-j-J^++2I-J+L-S-2s+3m_F+m_{J^+}+2m_J} \times \begin{pmatrix} I & J & F \\ m_I & m_J & -m_F \end{pmatrix}\begin{pmatrix} L & S & J \\ m_L & m_S & -m_J \end{pmatrix}\begin{pmatrix} L^+ & \ell & L \\ m_{L^+} & m_\ell & -m_L \end{pmatrix}\begin{pmatrix} S^+ & s & S \\ m_{S^+} & m_s & -m_S \end{pmatrix} \times \begin{pmatrix} F^+ & j & F \\ m_{F^+} & m_j & -m_F \end{pmatrix}\begin{pmatrix} \ell & s & j \\ m_\ell & m_s & -m_j \end{pmatrix}\begin{pmatrix} I & J^+ & F^+ \\ m_I & m_{J^+} & -m_{F^+} \end{pmatrix}\begin{pmatrix} L^+ & S^+ & J^+ \\ m_{L^+} & m_{S^+} & -m_{J^+} \end{pmatrix} \quad (14)$$

for any value of m_F. Whereas the transformation matrix $U_{i\alpha}$ for $I=0$ isotopes is block diagonal in J, the transformation matrix $U_{i_F\alpha_F}$ can be separated into individual F blocks, of which the $F=9/2$ matrix, with dimension 16×16, is the largest. Assuming that the eigenchannel quantum defects μ_α are equal for all isotopes and that the hyperfine interaction is negligible for the close-coupling region, the eigenchannel quantum defects μ_α obtained from the analysis of the Rydberg levels of an $I=0$ isotope and the $V_{\bar{\alpha}\alpha}$ matrix elements can also be used for the analysis of $I>0$ isotopes, i.e., $\mu_{\alpha_F}=\mu_\alpha$ and $V_{\bar{\alpha}_F\alpha_F}=V_{\bar{\alpha}\alpha}$. This requires that the signs of the elements of the corresponding frame transformation matrices of the different J values are consistent, which can be ensured by calculating the elements $U_{i\bar{\alpha}}=\langle LSJ|J^+jJ\rangle$ with Eq. (14) and setting $I=0$ and thus $F^+=J^+$ and $F=J$. Note that the resulting $U_{i\bar{\alpha}}$ matrices differ from those used by Aymar *et al.* [39] or those given by Condon and Shortley [54].

IV. RESULTS

For the initial millimeter-wave experiments, the tunable dye laser was set to excite krypton to the high-frequency end of the $58p$ or $60p$ Rydberg states (the levels "a"–"e" of ^{83}Kr in Table I) [see Fig. 1(a)]. The transitions to the np $[3/2]_J$ $(J=1,2)$ states of ^{84}Kr are located at the low-frequency edge of the bandwidth of the dye laser; thus only weak millimeter-wave transitions of ^{84}Kr were observed in the ^{84}Kr mass channel with no appreciable leaking into the ^{83}Kr mass channel [see Fig. 1(b)]. Typical overview spectra for ^{83}Kr are shown in Figs. 3 and 4. Transitions have been assigned using combination differences and the general $\Delta F=0,\pm1$ selection rule ($\Delta J=0,\pm1$ for ^{84}Kr). The assignment of the intermediate $n\ell[K]_J$ quantum numbers for ns and nd Rydberg levels of ^{83}Kr is based on the correlation, depicted in Fig. 5, to hyperfine levels of low-n states ($n\approx40$), where the hyperfine splitting is smaller than the separation between the individual $n\ell[K]_J$ levels.

The observed np, ns, and nd Rydberg levels of ^{84}Kr and ^{83}Kr are summarized in Tables I–III and their relative positions could be determined with an accuracy better than 1 MHz. ns and nd Rydberg states of ^{84}Kr with $J\leqslant3$ are accessible by the excitation scheme used in our experiment. The energies of the observed states relative to the $(4p)^6\,{}^1S_0$ ground state have been obtained by combining the present results with previous high-resolution laser data for $J=1$ states [5,32,33]; for the $J=2,3$ states, only data of moderate resolution for levels with $n<65$ are available [23,30]. In the case of ^{83}Kr, states with $3/2\leqslant F\leqslant15/2$ are accessible, but no transition involving nd states with $F=15/2$ or np states with $F=13/2$ has been identified. The energies of the observed states relative to the $(4p)^6\,{}^1S_0$ $F=9/2$ ground state have been obtained by combining the present results with the high-resolution laser data of Ref. [5].

TABLE I. *np* Rydberg states of ^{84}Kr and ^{83}Kr observed by millimeter-wave spectroscopy. The energies/h (MHz) are given relative to the position of the $70s\,[3/2]_2$ level ($F=13/2$ hyperfine level for ^{83}Kr). The positions of the $70s\,[3/2]_2$ level of ^{84}Kr and the $70s\,[3/2]_2$ ($F=13/2$) level of ^{83}Kr above the $^1S_0$ ground state are 112 889.913(16) and 112 889.855(16) cm^{-1}, respectively.

		n			
$n\ell\,[K]_J$	F	58	60	61	62
			^{84}Kr		
$np\,[3/2]_2$		−336133.6	−262802.6		
$np\,[3/2]_1$			−263098.3		
$np\,[1/2]_1$			−264916.9	−230938.6	
			^{83}Kr		
np "a"	5/2	−333583.8	−260248.3		
np "b"	7/2	−333628.8	−260281.5		
np "c"	9/2	−333919.4	−260570.4		
np "d"	7/2	−334180.1	−260799.9		
np "e"	11/2	−334292.3	−260930.4		
np "z"	11/2		−264619.9	−230650.5	−198383.6

The theoretical values of the bound levels probed by millimeter-wave experiments were calculated with a precision of 3 MHz (^{84}Kr) or 0.6 MHz (^{83}Kr), respectively. Because of the large number of parameters and correlations between parameters, some parameters, in particular the energy dependence of the quantum defects and several Euler angles θ_{jk}, have been fixed to literature values or set to zero. For example, for the interactions between the *LS*-coupled eigenchannels $p^5\ell\ ^{2S+1}L_J$, only interactions between channels differing in a single quantum number (either ℓ, S, or L) were considered. The restriction $\Delta L=0,\pm1$ has been applied, because the spin-orbit interaction has been considered as the main source for the deviation of the eigenchannels from purely *LS*-coupled channels and because the spin-orbit interaction matrix elements $\langle L'S'J|\Sigma_i\xi(r_i)\vec{\ell}_i\cdot\vec{s}_i|LSJ\rangle$ vanish un-

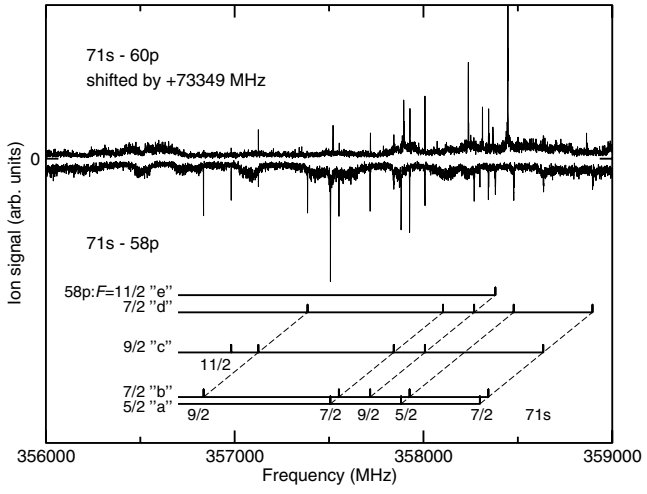

FIG. 3. Comparison of millimeter-wave overview spectra of the $71s\leftarrow58p$ (lower, inverted trace) and $71s\leftarrow60p$ (upper trace) transitions of ^{83}Kr. Lines with the same frequency shift share the same intermediate $58p/60p$ levels; e.g., 73 349 MHz is the difference between the $60p$ and $58p$ "c" ($F=9/2$) levels.

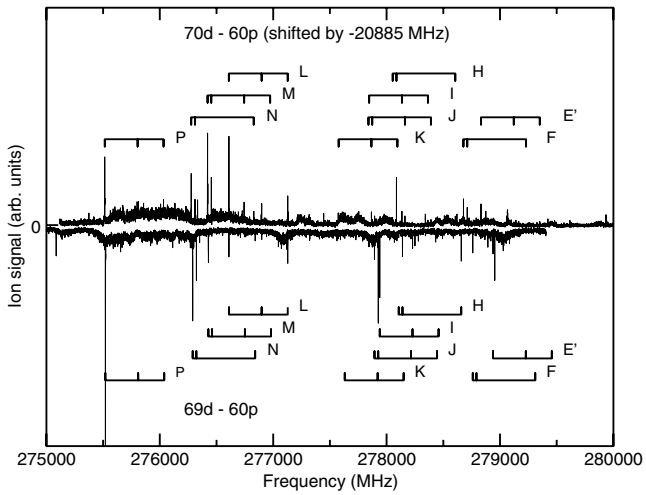

FIG. 4. Comparison of millimeter-wave overview spectra of the $69d\leftarrow60p$ and $70d\leftarrow60p$ transitions of ^{83}Kr. The capital letters stand for the following final states: E′ $nd\,[5/2]_2\,F=9/2$, F $nd\,[7/2]_3\,F=5/2$, H $nd\,[7/2]_4\,F=5/2$, I $nd\,[7/2]_3\,F=9/2$, J $nd\,[7/2]_4\,F=7/2$, K $nd\,[7/2]_4\,F=9/2$, L $nd\,[3/2]_2\,F=9/2$, M $nd\,[3/2]_2\,F=7/2$, N $nd\,[3/2]_2\,F=5/2$, P $nd\,[1/2]_1\,F=9/2$. Depending on the F value of the final state, each final state can be accessed from up to four different intermediate $60p$ hyperfine levels, causing typical line intervals indicated by the assignment bars (not all the lines are visible in the present spectra). The frequency shift of the $70d\,[3/2]_2\,F=9/2$ level with respect to the $69d\,[3/2]_2\,F=9/2$ level is 20 885 MHz.

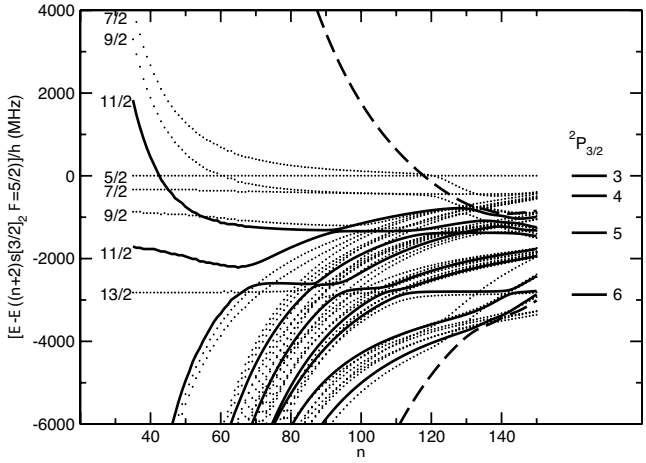

FIG. 5. Hyperfine structure of the $(n+2)s$ ($35\leqslant n\leqslant150$) Rydberg states of ^{83}Kr and of the $^2P_{3/2}$ state of ^{83}Kr$^+$, labeled with the value of F^+, as derived from the MQDT analysis. The $F=11/2$ levels are highlighted by the solid black curves. For $n>60$, avoided crossings due to interactions between $(n+2)s$ and nd hyperfine levels can be observed. For $n>120$, the hyperfine levels mix with those of the next higher or lower n, indicated by the broad dashed lines representing the lowest $F=11/2$ level of $(n+1)d/(n+3)s$ and the highest $F=11/2$ level of $(n-1)d/(n+1)s$, respectively.

TABLE II. *ns* and *nd* Rydberg states of ^{84}Kr observed by millimeter-wave spectroscopy. The energies/h (MHz) are relative to the 70*s* $[3/2]_2$ level. The differences between observed and calculated energies $(E_o-E_c)/h$ (MHz) are given in parentheses. The position of the 70*s* $[3/2]_2$ level of ^{84}Kr with respect to the $^1S_0$ ground state is 112 889.913(16) cm^{-1}.

	n						
$n\ell\ [K]_J$	68	69	70	71	72	73	74
$(n+2)s\ [3/2]_1$	547.9 (0.6)	22018.5 (0.1)	42561.7 (−1.3)	62229.8 (0.4)	81071.4 (0.2)	99132.8 (−0.8)	116456.4 (−2.3)
$(n+2)s\ [3/2]_2$	0.0 (1.3)	21494.8 (1.0)	42060.0 (0.6)	61749.3 (−0.4)	80611.3 (−1.3)	98691.8 (−1.1)	116033.4 (0.4)
$nd\ [3/2]_1$		20004.2 (0.5)					
$nd\ [5/2]_3$	−3936.0 (1.6)	17729.9 (1.6)	38456.9 (1.0)	58298.9 (−0.2)	77304.9 (2.0)		
$nd\ [5/2]_2$	−4856.8 (1.1)	16848.9 (1.9)	37613.1 (−0.4)	57489.9 (0.2)	76528.9 (−0.5)		
$nd\ [7/2]_3$	−5865.1 (0.2)	15885.3 (0.7)	36691.4 (1.3)	56607.9 (2.6)	75684.4 (0.4)		
$nd\ [7/2]_4$							
$nd\ [3/2]_2$	−7595.1 (−3.0)	14228.2 (−1.6)	35103.5 (−0.7)	55085.5 (0.1)	74223.9 (2.8)		
$nd\ [1/2]_1$	−8059.6 (0.3)	13785.8 (−0.3)	34682.0 (0.4)	54684.0 (0.4)	73841.4 (1.1)		
$nd\ [1/2]_0$							

less $\Delta\ell=0$, $\Delta L=0,\pm1$ and $\Delta S=0,\pm1$ [54,55]. The mixing of the *s* and *d* eigenchannels can be understood as an effect of short-range electrostatic interactions, i.e., quadrupole and exchange interactions, and occurs between channels with the same values of L and S [56].

The close-coupling channel parameters μ_α and $V_{\bar{\alpha}\alpha}$ (expressed in terms of the generalized Euler angles θ_{jk}) obtained in the fit and the transformation matrix $U_{i\alpha}$ for the $I=0$ isotopes are listed in Table IV. The remaining parameters and results of the MQDT analysis are summarized in Table V. Table III and Fig. 6 provide an overview of the comparison between the calculated and measured positions of the hyperfine components of the *ns* and *nd* Rydberg levels of ^{83}Kr, and the corresponding data on ^{84}Kr are listed in Table II. In Fig. 6 the calculated energies have been connected by a solid line for $F=11/2$ and dashed lines for other F values.

V. DISCUSSION AND CONCLUSIONS

The present MQDT model reproduces the hyperfine structure of high-n Rydberg states of ^{83}Kr including the avoided crossing between the $F=11/2$ levels of $(n+2)s\ [3/2]_2$ and $nd[3/2]_1$ to within typically 0.6 MHz (i.e., within measurement accuracy; see Table III). This indicates that the model chosen in Ref. [5], with a common set of close-coupling channel parameters for all isotopes and one set of hyperfine parameters for ^{83}Kr$^+$, is adequate to describe the hyperfine structure of high-n Rydberg states and to derive the hyperfine structure of the ion core. As can be seen in Fig. 5, the *ns* and the *nd* hyperfine levels reflect the overall hyperfine structure of the ion for $n>120$, but the details of the structure are obscured because the separation between the $n\ell[K]_JF$ and $(n+1)\ell[K]_JF$ levels becomes smaller than the width of the hyperfine structure of the ion $\Delta E_{\rm hf}=E(F^+=3)-E(F^+=6)$ for $n>130$. Whenever the separation $\Delta E_{\rm hf}$ between two hyperfine components of the ion becomes equal to the spacing between the n and $n+k$ Rydberg states, a condition that can be expressed as $\Delta E_{\rm hf}\approx k(2R_M/\nu_{\rm eff}^3)$, lines associated with different hyperfine series overlap in high-resolution spectra of very high Rydberg states resulting in a stroboscopic effect [57], as has been shown for the Rydberg series of ^{129}Xe and ^{131}Xe [6]. In the Rydberg series of ^{83}Kr, the present analysis confirms that this is the case for $\nu_{3/2}\approx133$ $(k=1)$ and $\nu_{3/2}\approx166$ $(k=2)$ (see also Fig. 4 of Ref. [5]).

In Sec. III, it has been assumed that the eigenchannels are nearly *LS* coupled. This is confirmed by the analysis of the present MQDT parameters (Table IV): The quantum defects μ_α are almost independent of the J value (as has already been noted by Aymar *et al.* [39]) and the Euler angles θ_{jk} which can be attributed to the spin-orbit interaction are small $(|\theta|\leqslant0.1)$. Only those Euler angles θ_{jk} which correspond to the *s*-*d* interaction $[\theta(d\ ^1P_1-s\ ^1P_1)\approx0.48$ and $\theta(d\ ^3P_J-s\ ^3P_J)\approx-0.14]$ are significant. Comparing the present MQDT parameters with those in the literature (see Table VI or Table 2 of Ref. [39]) shows that the absolute values of the Euler angles or the transformation matrix elements $U_{i\alpha}$ are similar to those obtained *ab initio* by Johnson *et al.* [38]. This is quite remarkable, because the present study is based on the analysis of the bound energy levels below the $^3P_{3/2}$ ionization limit as in the case of the study by Aymar *et al.* [39], whereas Johnson *et al.* [38] have analyzed the autoionizing resonances between the $^3P_{3/2}$ and $^3P_{1/2}$ ionization limits; the energy dependences of the eigenchannel quantum defects μ_α^1 of these two studies, however, are similar. Differences among the signs in Table VI result from the fact that the evaluated data are not sensitive to the sign of θ [e.g., for $\theta(d\ ^3P_0-s\ ^3P_0)$ and $\theta(d\ ^3P_2-s\ ^3P_2)$], or from different relative signs of the elements of the geometrical transformation matrix $U_{i\bar{\alpha}}$. In Table VI, the *s*-*d* channel interaction parameters of krypton are compared to those of other rare gases. Despite significant differences between the results of different studies, these parameters show a tendency to increase with increasing nuclear charge. For xenon, it is not possible to derive useful values for $\theta(d\ ^1P_1-s\ ^1P_1)$ and $\theta(d\ ^3P_1-s\ ^3P_1)$ because the $s\ ^1P_1$ and $s\ ^3P_1$ eigenchannels are strongly mixed [37,38,50].

For low n values, the MQDT predictions using eigenchannel quantum defects μ become worse because of (1) the

TABLE III. Hyperfine structure of *ns* and *nd* Rydberg states of ^{83}Kr observed by millimeter-wave spectroscopy. The energies/h (MHz) are relative to the $70s\ [3/2]_2$, $F=13/2$ level. The differences between observed and calculated energies $(E_o-E_c)/h$ (MHz) are given in parentheses. Only levels with $3/2 \leqslant F \leqslant 13/2$ have been observed. The position of the $70s\ [3/2]_2$, $F=13/2$ level with respect to the $^1S_0$ ground state is 112 889.865(16) cm^{-1}.

		n						
$n\ell\ [K]_J$	F	68	69	70	71	72	73	74
$(n+2)s\ [3/2]_1$	7/2	3241.6 (0.0)	24715.2 (0.0)	45260.7 (0.1)	64931.0 (−0.1)			
$(n+2)s\ [3/2]_1$	9/2	2610.1 (0.4)	24088.5 (0.5)	44638.9 (0.1)	64314.0 (−0.1)	83162.7 (0.0)	101230.9 (−0.3)	118561.1 (−0.5)
$(n+2)s\ [3/2]_1$	11/2	1575.5 (0.1)	23061.9 (−0.2)	43620.6 (−0.1)	63302.7 (0.0)	82157.6 (−1.4)	100233.6 (0.1)	117569.5 (−0.4)
$(n+2)s\ [3/2]_2$	5/2	2803.1 (−0.8)	24297.8 (−1.2)	44863.6 (−0.7)	64553.1 (−0.9)			
$(n+2)s\ [3/2]_2$	7/2	2430.7 (0.3)	23923.4 (−0.4)	44487.1 (−0.6)	64175.0 (0.0)			
$(n+2)s\ [3/2]_2$	9/2	1718.3 (0.3)	23206.1 (0.1)	43764.9 (0.3)	63447.6 (−0.1)	82303.1 (−0.4)		
$(n+2)s\ [3/2]_2$	11/2	637.1 (−0.5)	22154.8 (−0.1)	42748.8 (−0.1)	62471.1 (0.1)	81369.2 (−0.7)	99488.4 (−0.4)	116869.8 (−1.0)
$(n+2)s\ [3/2]_2$	13/2	0.0 (0.9)	21495.9 (1.1)	42062.6 (0.8)	61753.3 (1.2)	80616.4 (0.7)	98698.4 (0.4)	116041.6 (0.6)
$nd\ [3/2]_1$	11/2	84.7 (1.0)			61915.1 (−1.3)	80790.6 (−1.3)		
$nd\ [3/2]_1$	9/2	2.7 (0.7)	21574.6 (0.1)	42214.5 (0.4)	61973.1 (−0.8)	80902.2 (−1.3)	99047.3 (−1.4)	116450.4 (−1.9)
$nd\ [3/2]_1$	7/2	−280.6 (0.3)		41930.6 (−0.4)				
$nd\ [5/2]_3$	3/2	−1505.8 (0.1)	20161.2 (0.5)	40889.7 (0.7)				
$nd\ [5/2]_3$	5/2	−1582.3 (−0.2)	20088.8 (0.0)	40820.4 (−0.2)	60667.0 (0.1)			
$nd\ [5/2]_3$	7/2	−1706.8 (0.0)	19965.7 (−0.2)	40699.0 (0.1)				
$nd\ [5/2]_3$	9/2	−1873.4 (0.0)	19802.0 (−0.2)	40538.1 (−0.1)	60388.8 (−0.5)			
$nd\ [5/2]_3$	11/2	−2099.2 (0.3)	19579.0 (−0.1)	40318.6 (−0.2)	60172.6 (0.3)			
$nd\ [5/2]_3$	13/2	−2441.3 (0.5)	19238.6 (0.0)	39979.8 (−0.1)	59835.0 (−0.2)			
$nd\ [5/2]_2$	5/2	−2449.1 (0.0)	19258.9 (0.0)	40025.9 (−0.9)				
$nd\ [5/2]_2$	7/2	−2782.0 (0.4)	18929.7 (0.0)	39701.6 (0.4)	59586.1 (0.2)			
$nd\ [5/2]_2$	9/2	−3063.1 (1.1)	18657.0 (1.2)	39435.9 (0.9)				
$nd\ [5/2]_2$	11/2		18322.1 (1.5)	39104.6 (1.2)				
$nd\ [5/2]_2$	13/2							
$nd\ [7/2]_3$	3/2		18705.2 (−0.3)	39511.7 (0.6)				
$nd\ [7/2]_3$	5/2		18511.0 (−0.2)	39314.4 (−0.1)	59227.7 (−0.2)			
$nd\ [7/2]_3$	7/2	−3587.8 (−0.7)	18150.7 (−0.8)	38945.4 (−0.3)	58849.5 (0.0)			
$nd\ [7/2]_3$	9/2	−4076.2 (−0.5)	17658.1 (−0.5)	38449.3 (−0.6)				
$nd\ [7/2]_3$	11/2	−4630.4 (0.1)	17110.0 (−0.6)	37909.6 (0.0)				
$nd\ [7/2]_3$	13/2	−5177.2 (0.0)		37399.4 (0.0)				
$nd\ [7/2]_4$	3/2		18001.2 (0.2)	38834.2 (0.0)				
$nd\ [7/2]_4$	5/2		17858.4 (0.7)	38690.5 (0.2)				
$nd\ [7/2]_4$	7/2	−4131.9 (0.7)	17645.0 (0.7)	38476.3 (0.6)				
$nd\ [7/2]_4$	9/2	−4426.4 (0.7)	17349.7 (0.4)	38180.5 (0.4)	58120.0 (0.8)			
$nd\ [7/2]_4$	11/2	−4826.8 (0.7)		37771.2 (−0.6)				
$nd\ [7/2]_4$	13/2	−5395.4 (0.0)						
$nd\ [3/2]_2$	5/2	−5779.1 (−0.5)	16041.0 (0.1)	36913.6 (0.5)	56892.8 (1.5)			
$nd\ [3/2]_2$	7/2	−5645.6 (−0.8)	16179.8 (−0.9)	37057.6 (−0.1)	57041.3 (0.7)			
$nd\ [3/2]_2$	9/2	−5505.4 (−0.3)	16327.9 (−0.3)	37212.7 (0.4)	57202.9 (0.4)			
$nd\ [3/2]_2$	11/2	−6035.9 (−0.7)	15780.6 (−0.1)	36647.0 (−0.4)	56619.0 (0.0)			
$nd\ [3/2]_2$	13/2	−6737.3 (−1.9)	15072.1 (−0.5)	35931.7 (−1.1)				
$nd\ [1/2]_1$	9/2	−6589.1 (0.1)	15239.1 (0.4)	36118.0 (1.1)	56102.0 (1.6)			
$nd\ [1/2]_1$	7/2	−7028.6 (0.1)	14804.5 (−0.1)	35688.9 (0.7)	55677.5 (0.4)			
$nd\ [1/2]_1$	11/2	−7441.9 (−1.3)	14388.9 (−0.8)	35271.1(−0.4)	55258.6(−0.1)			
$nd\ [1/2]_0$	9/2	−7922.3 (−0.9)	13921.4(−0.7)	34817.0 (0.7)	54817.0 (0.9)			

TABLE IV. MQDT parameters for Kr.

	$\bar{\alpha}, i, \alpha$	1	2	3	4	5
$J=0$	$\bar{\alpha}$	$p^5d\,^3P_0$	p^5s $^3P_0$			
	i	$[^2P_{3/2}]d_{3/2}$	$[^2P_{1/2}]s_{1/2}$			
	μ_α^0	0.47412(17)	0.10380			
	μ_α^1	−0.430	0.271			
	$U_{i\alpha}$	0.9882	0.1534			
		−0.1534	0.9882			
	θ_{jk}		−0.1540			
$J=1$	$\bar{\alpha}$	$p^5d\,^1P_1$	$p^5d\,^3P_1$	$p^5d\,^3D_1$	$p^5s\,^1P_1$	$p^5s\,^3P_1$
	i	$[^2P_{3/2}]d_{5/2}$	$[^2P_{3/2}]d_{3/2}$	$[^2P_{1/2}]d_{3/2}$	$[^2P_{3/2}]s_{1/2}$	$[^2P_{1/2}]s_{1/2}$
	μ_α^0	0.09125(46)	0.47039(11)	0.26585(32)	0.05930(33)	0.11055(60)
	μ_α^1	0.073	−0.515	−0.844	0.121	0.269
	$U_{i\alpha}$	0.6773	−0.5418	−0.3381	−0.3595	−0.0641
		0.2389	0.7429	−0.6033	−0.1219	0.1104
		0.5166	0.3669	0.7223	−0.2701	0.0622
		0.3806	−0.0815	0.0000	0.7428	0.5447
		−0.2692	−0.1152	0.0000	−0.4808	0.8265
	θ_{jk}		0.0162(12)	0.0	0.4850(17)	0.0
				−0.0395(16)	0.0	−0.1416(18)
					0.0	0.0
						0.0367(10)
$J=2$	$\bar{\alpha}$	$p^5d\,^3P_2$	$p^5d\,^3D_2$	$p^5d\,^3F_2$	$p^5d\,^1D_2$	$p^5s\,^3P_2$
	i	$[^2P_{3/2}]d_{5/2}$	$[^2P_{3/2}]d_{3/2}$	$[^2P_{1/2}]d_{3/2}$	$[^2P_{1/2}]d_{5/2}$	$[^2P_{3/2}]s_{1/2}$
	μ_α^0	0.46544(8)	0.27089(82)	0.38526(48)	0.29276(78)	0.09946(12)
	μ_α^1	−0.650	−0.829	−0.950	−0.695	0.213
	$U_{i\alpha}$	0.6442	−0.2992	−0.1739	0.6771	0.0830
		−0.2842	0.6958	−0.4696	0.4617	−0.0366
		−0.1412	0.2175	0.8534	0.4518	−0.0182
		0.6841	0.6156	0.1448	−0.3525	0.0881
		−0.1278	0.0000	0.0000	0.0000	0.9918
	θ_{jk}		−0.0051(6)	0.0	0.0	−0.1281(7)
				0.0523(11)	−0.0207(15)	0.0
					0.0	0.0
						0.0
$J=3$	$\bar{\alpha}$	$p^5d\,^3D_3$	$p^5d\,^3F_3$	$p^5d\,^1F_3$		
	i	$[^2P_{3/2}]d_{5/2}$	$[^2P_{3/2}]d_{3/2}$	$[^2P_{1/2}]d_{5/2}$		
	μ_α^0	0.29154(36)	0.39654(14)	0.26023(75)		
	μ_α^1	−0.780	−0.809	−0.780		
	$U_{i\alpha}$	0.8495	−0.0529	0.5249		
		−0.2932	0.7797	0.5532		
		0.4386	0.6239	−0.6469		
	θ_{jk}		−0.0484(7)	0.0		
				0.1058(10)		
$J=4$	$\bar{\alpha}$	$p^5d\,^3F_4$				
	i	$[^2P_{3/2}]d_{5/2}$				
	μ_α^0	0.39843(12)				
	μ_α^1	−0.659				

TABLE V. MQDT results for Kr.

	^{84}Kr	^{83}Kr		
R_M (cm^{-1})	109736.5979	109736.5892		
$E(^2P_{3/2})$ (cm^{-1})	112914.4340[a,c]	112914.4336[b,c]		
$E(^2P_{1/2})$ (cm^{-1})	118284.50[d]	118284.50[d]		
$E(^2P_{3/2})-E_{\mathrm{ref}}$[e] (cm^{-1})	24.52120(8)	24.56809(8)		
$A_{3/2}$ (cm^{-1})		−0.00661(3)	−0.00616(4)[f]	−0.006194[g]
$B_{3/2}$ (cm^{-1})		−0.0154(7)	−0.0127(4)[f]	−0.0138[g]
$A_{1/2}$ (cm^{-1})		−0.04[b]		
$\sigma_{\mathrm{mm\ wave}}$ (MHz)	1.2	0.6		

[a]Fixed to the value from Ref. [32].
[b]Fixed to the value from Ref. [5].
[c]Uncertainty in the vuv calibration 0.016 cm^{-1}.
[d]Fixed to the value from Ref. [23].
[e]The reference level E_{ref} is $70s\ [3/2]_2$ (or its $F=13/2$ hyperfine level for ^{83}Kr).
[f]From Ref. [5].
[g]*Ab initio* result from Ref. [53].

energy dependence of the MQDT parameters as mentioned above and (2) the existence of unphysical solutions of the MQDT equation (corresponding to nonexistent d states). Such spurious solutions do not occur when η quantum defects are used instead of μ defects; moreover, η defects normally tend to be less energy dependent [46,47,58]. A global analysis of all observed ns and nd levels of krypton, including the low-n states as well as the autoionizing levels lying between the $^2P_{3/2}$ and $^2P_{1/2}$ ionization thresholds and using η defects, will be described elsewhere [48].

The hyperfine structure of the $^2P_{3/2}$ state of the ion determined in the present study is summarized in Table V. The quoted errors are estimated from the results of different fits and are much larger than the standard deviations of the final fit. The hyperfine structure of the present study has slightly larger values of A and B than the structure determined in Ref. [5] (and the similar theoretical values of Ref. [53]), which results in slightly larger separations between the lower three hyperfine levels ($F^+=6,5,4$) of the ion. This discrepancy may be explained by the fact that Wörner *et al.* [5] fitted A and B only to the hyperfine levels of the $ns\ [3/2]_1$ Rydberg series, which converge to the upper three hyperfine levels ($F^+=5,4,3$) of the ion (see Fig. 5), and to the perturbed $F=11/2$ levels of the $ns\ [3/2]_2$ Rydberg series. The results shown in Table V illustrate the power of the combination of high-resolution millimeter-wave spectroscopy of Rydberg states and MQDT to determine the hyperfine structure of cations.

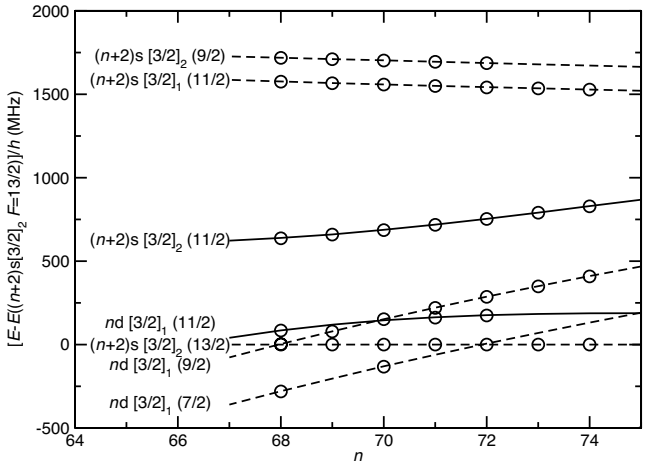

FIG. 6. Hyperfine structure of high-n Rydberg states of ^{83}Kr: experimental values are indicated with circles and lines connect the calculated level positions. The avoided crossing between the $F=11/2$ levels of $(n+2)s[3/2]_2$ and $nd[3/2]_1$ is marked with solid lines. The size of the circles does not represent the uncertainty of the experimental measurements, which is better than 1 MHz.

TABLE VI. s-d channel interaction parameters for rare gas atoms expressed as generalized Euler angles θ (rad).

	$^1P_1$	$^3P_0$	$^3P_1$	$^3P_2$	
Ne	0.032	0.0374	−0.051		[a]
Ar	−0.02		−0.18		[b]
	0.042		0.097		[c]
Kr	0.485	−0.154	−0.142	−0.128	[d]
	−0.495		0.148		[c]
	0.0	0.172	−0.102	0.12	[e]
	0.018		0.080		[f]
Xe		0.1065			[g]

[a]Reference [45].
[b]*Ab initio* values from Ref. [56].
[c]Derived from the $U_{i\alpha}$ matrix of Ref. [38] based on *ab initio* values.
[d]This study.
[e]Derived from the $U_{i\alpha}$ matrix of Ref. [39].
[f]Derived from the $U_{i\alpha}$ matrix of Ref. [37].
[g]Reference [59].

ACKNOWLEDGMENTS

The authors thank Gregory M. Greetham for his help during the first stage of the experiment and Hans Jakob Wörner (ETH Zürich) and Christian Jungen (Orsay) for helpful discussions concerning the MQDT calculations. This work is supported by ETH Zürich (Project No. TH 29/04-3) and the Swiss National Science Foundation (Project No. NF 200020-108080/1).

[1] A. Osterwalder, A. Wüest, F. Merkt, and Ch. Jungen, J. Chem. Phys. **121**, 11810 (2004).
[2] T. Trickl, M. J. J. Vrakking, E. Cromwell, Y. T. Lee, and A. H. Kung, Phys. Rev. A **39**, 2948 (1989).
[3] F. Brandi, W. Hogervorst, and W. Ubachs, J. Phys. B **35**, 1071 (2002).
[4] Th. A. Paul and F. Merkt, J. Phys. B **38**, 4145 (2005).
[5] H. J. Wörner, U. Hollenstein, and F. Merkt, Phys. Rev. A **68**, 032510 (2003).
[6] H. J. Wörner, M. Grütter, E. Vliegen, and F. Merkt, Phys. Rev. A **71**, 052504 (2005).
[7] C. Fabre, P. Goy, and S. Haroche, J. Phys. B **10**, L183 (1977).
[8] T. F. Gallagher, *Rydberg Atoms* (Cambridge University Press, Cambridge, UK, 1994).
[9] F. Merkt and A. Osterwalder, Int. Rev. Phys. Chem. **21**, 385 (2002).
[10] C. Fabre, S. Haroche, and P. Goy, Phys. Rev. A **18**, 229 (1978).
[11] P. Goy, C. Fabre, M. Gross, and S. Haroche, J. Phys. B **13**, L83 (1980).
[12] F. Merkt and H. Schmutz, J. Chem. Phys. **108**, 10033 (1998).
[13] F. Merkt, R. Signorell, H. Palm, A. Osterwalder, and M. Sommavilla, Mol. Phys. **95**, 1045 (1998).
[14] A. Osterwalder and F. Merkt, Phys. Rev. Lett. **82**, 1831 (1999).
[15] M. Schäfer, M. Andrist, H. Schmutz, F. Lewen, G. Winnewisser, and F. Merkt, J. Phys. B **39**, 831 (2006).
[16] A. Osterwalder, S. Willitsch, and F. Merkt, J. Mol. Struct. **599**, 163 (2001).
[17] A. Osterwalder, R. Seiler, and F. Merkt, J. Chem. Phys. **113**, 7939 (2000).
[18] C. E. Moore, *Atomic Energy Levels*, Circular 467/2 (U.S. GPO, Washington D.C., 1952).
[19] V. Kaufman and C. J. Humphreys, J. Opt. Soc. Am. **59**, 1614 (1969).
[20] K. Yoshino and Y. Tanaka, J. Opt. Soc. Am. **69**, 159 (1979).
[21] C. Delsart, J.-C. Keller, and C. Thomas, J. Phys. B **14**, 3355 (1981).
[22] C. Delsart, J.-C. Keller, and C. Thomas, J. Phys. B **14**, 4241 (1981).
[23] J. Sugar and A. Musgrove, J. Phys. Chem. Ref. Data **20**, 859 (1991).
[24] D. Klar, K. Harth, J. Ganz, T. Kraft, M.-W. Ruf, H. Hotop, V. Tsemekhman, K. Tsemekhman, and M. Ya. Amusia, Z. Phys. D: At., Mol. Clusters **23**, 101 (1992).
[25] M. Bounakhla, J. P. Lemoigne, J. P. Grandin, X. Husson, H. Kucal, and M. Aymar, J. Phys. B **26**, 345 (1993).
[26] V. Kaufman, J. Res. Natl. Inst. Stand. Technol. **98**, 717 (1993).
[27] K. Maeda, K. Ueda, and K. Ito, J. Phys. B **26**, 1541 (1993).
[28] S. M. Koeckhoven, W. J. Buma, and C. A. de Lange, Phys. Rev. A **49**, 3322 (1994).
[29] S. M. Koeckhoven, W. J. Buma, and C. A. de Lange, Phys. Rev. A **51**, 1097 (1995).
[30] S. Yoon and W. L. Glab, J. Phys. B **27**, 4133 (1994).
[31] D. Klar, M. Aslam, M. A. Baig, K. Ueda, M.-W. Ruf, and H. Hotop, J. Phys. B **34**, 1549 (2001).
[32] U. Hollenstein, R. Seiler, and F. Merkt, J. Phys. B **36**, 893 (2003).
[33] U. Hollenstein, Ph.D. thesis, Eidgenössische Technische Hochschule Zürich, 2003 (unpublished).
[34] T. Peters, T. Halfmann, U. Even, A. Wünnenberg, I. D. Petrov, V. L. Sukhorukov, and H. Hotop, J. Phys. B **38**, S51 (2005).
[35] R. Silwal and J. R. Brandenberger, Phys. Rev. A **73**, 032508 (2006).
[36] K. T. Lu and U. Fano, Phys. Rev. A **2**, 81 (1970).
[37] J. Geiger, Z. Phys. A **282**, 129 (1977).
[38] W. R. Johnson, K. T. Cheng, K.-N. Huang, and M. Le Dourneuf, Phys. Rev. A **22**, 989 (1980).
[39] M. Aymar, O. Robaux, and C. Thomas, J. Phys. B **14**, 4255 (1981).
[40] A. L'Huillier, X. Tang, and P. Lambropoulos, Phys. Rev. A **39**, 1112 (1989).
[41] E. Audouard, P. Laporte, J.-L. Subtil, N. Damany, and M. Pellarin, Phys. Rev. A **41**, 6032 (1990).
[42] J. Z. Wu, S. B. Whitfield, C. D. Caldwell, M. O. Krause, P. van der Meulen, and A. Fahlman, Phys. Rev. A **42**, 1350 (1990).
[43] K. Ito, H. Masuda, Y. Morioka, and K. Ueda, Phys. Rev. A **47**, 1187 (1993).
[44] M. Ahmed, M. A. Zia, M. A. Baig, and B. Suleman, J. Phys. B **30**, 2155 (1997).
[45] K. Harth, M. Raab, J. Ganz, A. Siegel, M.-W. Ruf, and H. Hotop, Opt. Commun. **54**, 343 (1985).
[46] M. J. Seaton, Mon. Not. R. Astron. Soc. **118**, 504 (1958).
[47] M. J. Seaton, Rep. Prog. Phys. **46**, 167 (1983).
[48] M. Schäfer, F. Merkt, and Ch. Jungen (unpublished).
[49] F. Merkt, A. Osterwalder, R. Seiler, R. Signorell, H. Palm, H. Schmutz, and R. Gunzinger, J. Phys. B **31**, 1705 (1998).
[50] K. T. Lu, Phys. Rev. A **4**, 579 (1971).
[51] C.-M. Lee and K. T. Lu, Phys. Rev. A **8**, 1241 (1973).
[52] J.-Q. Sun, Phys. Rev. A **40**, 7355 (1989).
[53] S. Fraga, K. M. S. Saxena, and B. W. N. Lo, At. Data **3**, 323 (1971).
[54] E. U. Condon and G. H. Shortley, *The Theory of Atomic Spectra* (Cambridge University Press, London, 1953).
[55] R. N. Zare, *Angular Momentum* (John Wiley & Sons, New York, 1988).
[56] C. M. Lee, Phys. Rev. A **10**, 584 (1974).
[57] P. Labastie, M. C. Bordas, B. Tribollet, and M. Broyer, Phys. Rev. Lett. **52**, 1681 (1984).
[58] Ch. Jungen (private communication).
[59] R. D. Knight, Phys. Rev. A **34**, 3809 (1986).